Nanotechnology **21** (2010) 045704 (7pp) doi:10.1088/0957-4484/21/4/045704

Engineering graphene by oxidation: a first-principles study

Zhiping Xu[1] **and Kun Xue**[2,3]

[1] Department of Civil and Environmental Engineering, Massachusetts Institute of Technology, Cambridge, MA 02139, USA
[2] Department of Engineering Mechanics, Tsinghua University, Beijing 100084, People's Republic of China
[3] State Key Laboratory of Explosion Science and Technology, Beijing Institute of Technology, Beijing 100084, People's Republic of China

E-mail: xuzp@mit.edu

Received 18 August 2009, in final form 9 November 2009
Published 16 December 2009
Online at stacks.iop.org/Nano/21/045704

Abstract
Graphene epoxide, with oxygen atoms lining up on pristine graphene sheets, is investigated theoretically here using first-principles calculations. Two distinct phases—metastable clamped and stable unzipped structures—are observed consistent with experimental observations. In the clamped structure, oxygen atoms form a regular lattice on the graphene sheet. In the unzipped phase, an epoxy group breaks the lower sp^2 bond and modifies the mechanical and electronic properties of graphene remarkably. The foldable epoxy ring structure reduces its Young's modulus by 42.4%, while leaving the tensile strength almost unchanged. The perturbation of epoxidation on the band structures depends on the density and symmetry of oxidation. These results pave the way for oxidation-based engineering of graphene-related materials.

1. Introduction

Recently developed techniques to isolate single-layer graphene from graphite [1] provides the possibility to investigate this extremely monolayer material. With a hexagonal graphitic lattice, graphene possesses exceptional properties such as massless Dirac fermions [2], abnormal quantum Hall effects [3], and extremely high stiffness and structural stability [4]. Besides the intrinsic properties of graphene, fresh physics has also been revealed in graphene-related nanostructures, such as that finite-width graphene nanoribbons feature half-metallicity [5] and patternable transport properties [6, 7]. One of the most convenient processes to obtain graphene materials is chemical exfoliation [8–10], where crystalline graphite is first exfoliated through oxidation and reduced to graphene monolayers subsequently. This method takes advantage of massive production and possible deposition from solution [11] in comparison to other approaches such as mechanical cleavage [1], epitaxial growth [12] and organic synthesis [13]. However, the products of the current technique contain a considerable amount of the intermediate product, graphene oxide, which has a large number of epoxy and hydroxyl groups and has a significant impact on its properties [14]. A previous study reports that incomplete reduction leaves wrinkles and folds in the graphene sheet products and is detrimental to the electronic properties [15].

Interest has also arisen for functional graphene materials such as graphene oxides [16–20]. Although these have been studied for decades, there is very limited knowledge on the atomic structure and the physical properties of the graphene oxides. Several atomic models have been proposed with different functional groups [17]. The most notable structure proposed is the Lerf–Klinowski model on the basis of NMR spectroscopy data [20], which contains epoxy and hydroxyl groups on the graphene sheets or at their edges. Fault lines in graphene are observed experimentally as a result of oxidation [18]. This is explained as adsorbed epoxy groups that tend to line up cooperatively. A recent ultrahigh vacuum scanning probe microscopy (UHV STM) study reveals locally periodic structures. The atomic structure is identified to be an oxygen atom lattice bound to the graphene sheet [19]. These oxidized monolayer sheets are structurally close to graphene and are expected to have similarly peculiar properties. One can thus functionalize graphene structures in a controllable manner through chemical oxidation and reduction [17, 21]. These features provide graphene epoxide with great potentials in material applications. For this purpose, a good understanding of their structural

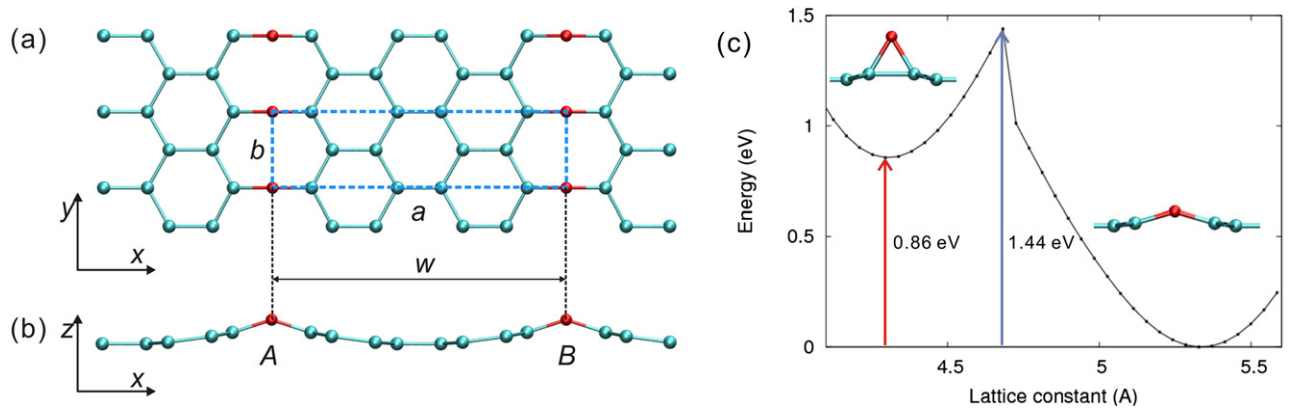

Figure 1. (a), (b) Optimized structure of graphene epoxide. Each unit cell (dashed rectangle) with width a and height b contains one oxygen atom (in red). The width w of the unit cell is defined as a multiple of the period of graphene unit cells. For the structure shown, $w = 2$. The epoxy group at neighboring sites A and B can be either in the same (*symmetric*) or opposite (*antisymmetric*) side of the graphene. (c) Energy landscape for graphene epoxide C_4O ($w = 1$) as changing the lattice constant along the x direction: insets shows its metastable clamped (left) and unzipped (right) structures, separated by a barrier of 0.58 eV.

(This figure is in colour only in the electronic version)

and electronic properties is urged. In this work, we will discuss their energetic, structural and electronic properties based on extensive first-principles calculations. Although experimental observation [22] concludes that graphite oxide is a disordered non-stoichiometric phase containing both epoxide and hydroxyl groups, we expect the structural properties relationship presented here for regularly patterned structures to shed some light on possible applications of this unique material.

In the Lerf–Klinowski model of graphene epoxide, oxygen atoms are covalently bonded to two neighboring carbon atoms in graphene, forming an epoxy ring group [20]. Optical image studies and energetic analysis show these epoxy groups like to form fault lines cooperatively, to lower their formation energy [18]. The adsorption of an epoxy group is found to be able to break the lower sp^2 carbon bonds and the process is described as oxygen-driven 'unzipping" of graphitic materials [18, 23]. On the other hand, recent scanning probe microscopy identifies periodic patterns of the oxygen atoms bound to the graphene sheet [19], where the oxygen lines are also aligned along the zigzag edges. Instead of breaking a carbon–carbon (C–C) bond in the unzipping mechanism, the C–C bond length and lattice constants in the periodic structures are very close to pristine graphene [19]. Inspired by these studies, we propose here a graphene epoxide model as depicted in figure 1 to probe their structure and properties. In this model, the epoxy groups line up in the y direction, and are patterned periodically along the x direction (armchair). We characterize the structure of the graphene epoxide using the unit cell shown in figure 1. The characteristic width of the unit cell w is defined in units of the graphene lattice period in the x direction. As an example, the unit cell shown in figures 1(a) and (b) has the width $w = 2$. Following this definition, the unit cell with width w has a chemical composition of one epoxy group and $4w$ carbon atoms, i.e. $C_{4w}O$ ($w = 1, 2, \ldots$), and is used to investigate the bulk properties of graphene oxides with a corresponding epoxidation density $1/(4w)$. It is also noticeable that the epoxy group can be adsorbed on either side of the graphene, so there are different configurations for $C_{4w}O$ according to the binding symmetry. Depending on which surface of the graphene is accessible for oxidation, the neighboring epoxy groups (A and B in figure 1) can be adsorbed on the same (antisymmetric phase, $C_{4w}O_{asym}$) or opposite side (symmetric phase, $C_{4w}O_{sym}$) of the graphene (see insets in figure 3).

2. Computational methods

The atomic structure of the graphene epoxide is constructed from pristine graphene by adding oxygen atoms on or below carbon atoms with an initial guess according to the epoxy ring structure. The optimized structure is determined then by a conjugated gradient-algorithm-based geometrical optimization on both the atom coordinates and cell sizes, through first-principles calculations. In our work, plane-wave basis-set-based density functional theory (DFT) is employed with a local (spin) density approximation (LDA) using the code PWSCF[4]. Ultrasoft pseudopotentials are used for ion–valence electron interactions [24]. For all the results presented here, energy cutoffs of 30 Ryd and 240 Ryd are used for plane-wave basis sets and charge density grids, respectively. The settings have been verified to achieve a total energy convergence less than 10^{-5} Ryd/atom. For variable-cell relaxation, the criteria for stress and force on atoms are set to be 0.01 GPa and 0.001 Ryd $Å^{-1}$. Eight Monkhorst–Pack k-points are used in each periodic direction for Brillouin zone integration, which is qualified for the energy convergence criteria of 3 meV. Although the DFT-LDA approaches are widely used for carbon nanostructures [5, 11, 25], we are also aware that advanced techniques such as hybrid-DFT methods [26] should be applied for improvements in accuracy.

[4] PWSCF (distributed in the Quantum-Espresso package) is a community project for high-quality quantum-simulation software, based on density functional theory, and coordinated by Paolo Giannozzi. See http://www.quantumespresso.org.

Table 1. Structural properties of symmetrical graphene epoxide with various oxygen density.

w	0.5 (c) [a]	0.5 (u) [a]	1 (c)	1 (u)	2 (u)	4 (u)	8 (u)	12 (u)
a (Å)	4.57	6.47	4.30	5.33	9.48	17.72	34.67	68.01
b (Å)	2.58	2.48	2.52	2.45	2.44	2.44	2.44	2.44
d_{C-C} (Å) [b]	1.50	2.58	1.49	2.55	2.53	2.51	2.51	2.53
A_{C-O-C} (deg)	63.9	153.6	62.3	148.2	144.6	142.1	142.9	146.2
ε_x^c	0.083	0.533	0.018	0.262	0.123	0.050	0.027	0.019

[a] (c) stands for clamped phase, (u) for unzipped phase.
[b] For graphene, $d_{C-C} = 1.408$ Å. d_{C-C} is the C–C distance underneath the oxygen atom. A_{C-O-C} is the C–O–C angle in the epoxy group.
[c] The x-direction strain is defined using lattice constants of pristine graphene as reference values.

3. Results and discussion

3.1. Atomic structures of graphene epoxide

The atomic structure of graphene epoxide discussed in this work is obtained after variable-cell geometric optimization. The result shows that the graphene sheet buckles around the epoxy groups. The structural distortion depends on the epoxide density $1/(4w)$, as summarized in table 1. For $w \leqslant 1$, there exists a metastable clamped phase (figure 1(c)) where the epoxy ring is close to an equilateral triangle. In these structures, the adsorption of an oxygen atom stretches the lower C–C bonds by 5% but does not break the sp^2 carbon network (figure 4(b)). However, this clamped phase is metastable. As we increase the lattice constant along the x direction, the graphene epoxide collapses into a more stable unzipped phase with a sp^2 bond underneath the oxygen atom broken. The energy difference is $E_{\text{clamped}} - E_{\text{unzipped}} = 0.86$ eV. A significant energy barrier between these two phases ($E_b = 0.58$ eV for $w = 1$, and 1.7 eV for $w = 0.5$) makes the clamped phase considerably more stable. For $w > 1$, the metastable clamped phase disappears, leaving the unzipped structure the only possible configuration. The angle C–O–C between two carbon–oxygen bonds in an unzipped epoxy ring is about 150°, and the final C–C bond is broken with an extended distance of 2.5 Å (figure 1(c)). The structure of the epoxy ring does not change much as the width w increases further, suggesting that strain energy induced by the local distortion decays quickly as the oxidation density decreases. This explains the folds and wrinkles observed in graphene oxides due to sparse epoxy lines [15]. Table 1 summarizes detailed structural information of various graphite epoxides.

Our result explains the discrepant observations of the graphene oxide structure in [18, 19]. (1) The periodic epoxy lattice observed in resolved STM images has lattice constants 2.73 Å (x) and 4.06 Å (y), which are comparable with a graphene sheet [19]. In our calculation, this structure corresponds to the clamped phase with $w = 1$. (2) The 'unzipping' mechanism for the epoxy line network is consistent with the unzipped phase observed here. The broken C–C bond in the epoxy group could give rise to the observable lines in optical microscopy [18]. We also simulate the STM images for symmetrical graphene oxides (both clamped and unzipped) from the local density of states around the Fermi energy [28], using a sample bias of 1 V. The result shown in figure 2 is consistent with Pandey's experimental observation [19]. In our results, the lattice constants for $w = 1$ as summarized in table 1 are $a = 2.52$ Å (x) and $b = 4.30$ Å (y), which are close to both Pandey *et al*'s STM observation and previous reports using neutral scattering [19, 27].

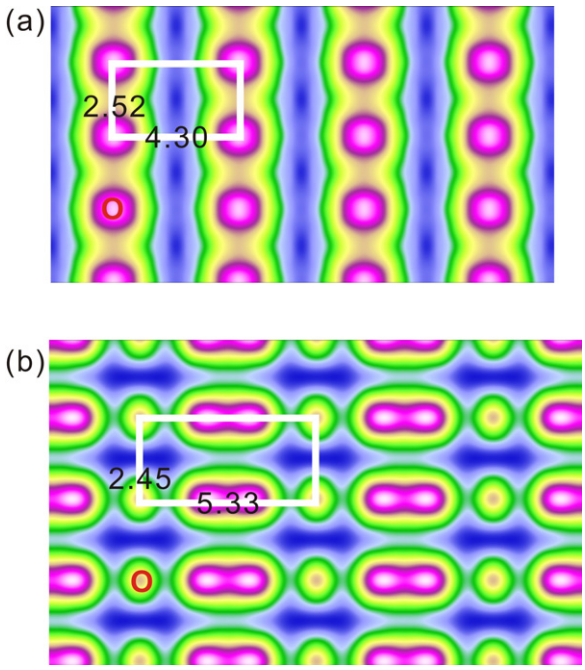

Figure 2. Simulated STM image for (a) clamped and (b) unzipped graphene oxide where epoxy groups bind on the same side. Position of oxygen atoms is denoted by 'O'. A sample bias of 1 V is applied and the position of the scanning tip is kept to be 2 Å higher than the oxygen atom. The unit cell and correspondence lattice constants are depicted. For the clamped phase, the simulated image and lattice constants ($a = 4.30$ Å and $b = 2.45$ Å) are consistent with experimental results [19].

As discussed before, if both sides of the graphene are accessible for oxidation, neighboring epoxy groups can reside on opposite sides to form the so-called antisymmetric structure. The formation energy of graphene epoxide in this symmetry is lower in unzipped phases. In the antisymmetric structures (lower inset, figure 3), the planar structure of the graphene between epoxy groups is well kept and there is negligible lattice distortion in the graphene sheet. The final structure is relaxed in a zigzag shape, where epoxy groups hinge planar zigzag graphene ribbons.

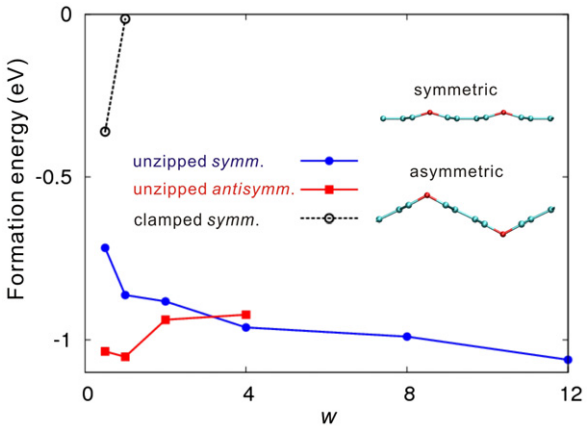

Figure 3. Formation energy of graphene epoxide with dependence on their structures and width w. The filled circles and squares stand for symmetrically/antisymmetrically unzipped structures. Open circles are symmetrically clamped structures, which are unstable for $w > 1$. The insets show the optimized structure of symmetric and antisymmetric structures for C_4O ($w = 1$), projected along the y direction.

3.2. Binding strength between epoxy group and graphene

The binding strength between the epoxy group and graphene sheet is characterized through the formation energy $E_f = E_{\text{graphene epoxide}} - (E_{\text{graphene}} + E_{\text{oxygen}}/2)$, where $E_{\text{graphene epoxide}}$ and E_{graphene} are the energy of graphene epoxide and pristine graphene. A negative value of E_f with larger amplitude means the oxidation is more favorable. The reference energy value for oxygen atoms is calculated from isolated O_2 molecules in the singlet state, i.e. $E_{\text{oxygen}}/2$. The results depicted in figure 3 show that the unzipped structure binds stronger with the graphene. In the clamped phase, the formation energy decreases as the oxidation density $1/(4w)$ increases as shown in figure 3 and [11, 16], while for unzipped structures, E_f increases because at elevated epoxy density the distortion of graphene is built up. When the width w increases to be larger than 2 for the unzipped structures, the distortion energy of graphene sheets is able to be released more effectively and the formation energy converges for large w. For $w > 12$, the formation energy approaches a value of $E_f = -1.06$ eV. This significant binding strength makes the epoxy group hard to be removed in the reduction process and thus prohibits high-quality synthesis for pristine graphene materials from graphene exfoliates [15]. In the antisymmetric structures, negligible strain is introduced in the graphene lattice; thus the energy of the epoxy group determines the binding strength that saturates at large w values.

3.3. Mechanical properties of graphene epoxide

The formation of the epoxy ring and breaking of the covalent sp^2 bond imply remarkable effects on the mechanical properties of graphene. To understand this effect, mechanical loading has been applied to the unit cell of both pristine graphene and graphene epoxide C_8O ($w = 2$). Uniaxial strain loading is applied by scaling both the lattice constant in the x direction and the atom coordinates simultaneously. The lattice constant in the y direction and atom coordinates are optimized afterward. Stresses are defined by considering the sheet has a thickness of 3.34 Å, which is the inter-layer distance in graphite crystals. The stress–strain relations are plotted in figure 4. It is found that epoxy groups soften the structure significantly, especially in compression. This comes from the flexibility of pre-stretched C–C bonds and foldable C–O–C angles. The epoxy ring is found to reduce the Young's modulus of graphene by 42.4% (from 1060 to 610 GPa) along the x direction and 9.63% (from 1061 to 960 GPa) in the y direction. At small strain the loading is born by the bending of the C–O–C angle rather than stretching and compression of sp^2 bonds in graphene. In contrast to the huge reduction in Young's modulus, the tensile strength of graphene epoxide along the x direction almost does not change (111 GPa), and elastic strain before breaking decreases from 0.20 to 0.18, consistent with previous molecular dynamics simulations [29]. As tensile loading is being applied along the x direction, the epoxy ring first bends into the graphene sheet plane. Then the structure starts to break after the in-plane bonds are elongated to their elastic limit (figure 4). The charge density distribution

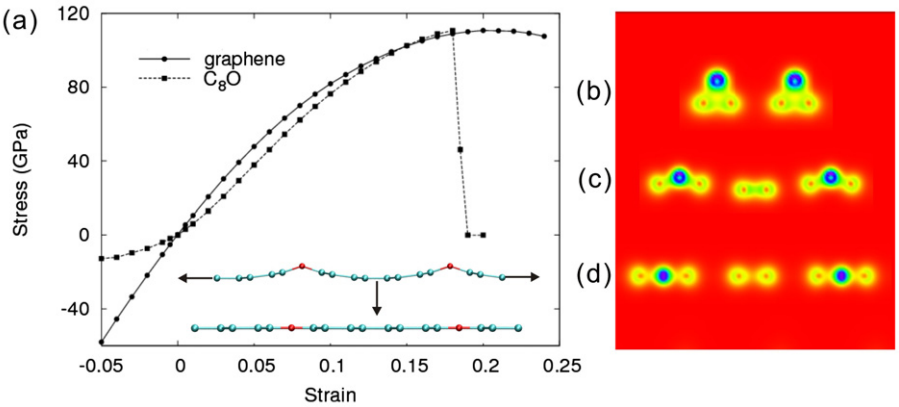

Figure 4. (a) Stress–strain relation of graphene and graphene epoxide. Insets: structural change under uniaxial strain from 0.0 to 0.18. (b)–(d) Charge density distribution of the epoxy ring, projected in the x–z plane along the y line containing oxygen atoms. Panel (b) shows the metastable clamped structure with C–C bond length at 1.5 Å ($w = 1$); (c) and (d) show the bending and flattening of C–O–C angle with strain 0.0 and 0.18 (at the breaking point), respectively, for $w = 2$. Blue (red) color stands for high (low) electron density.

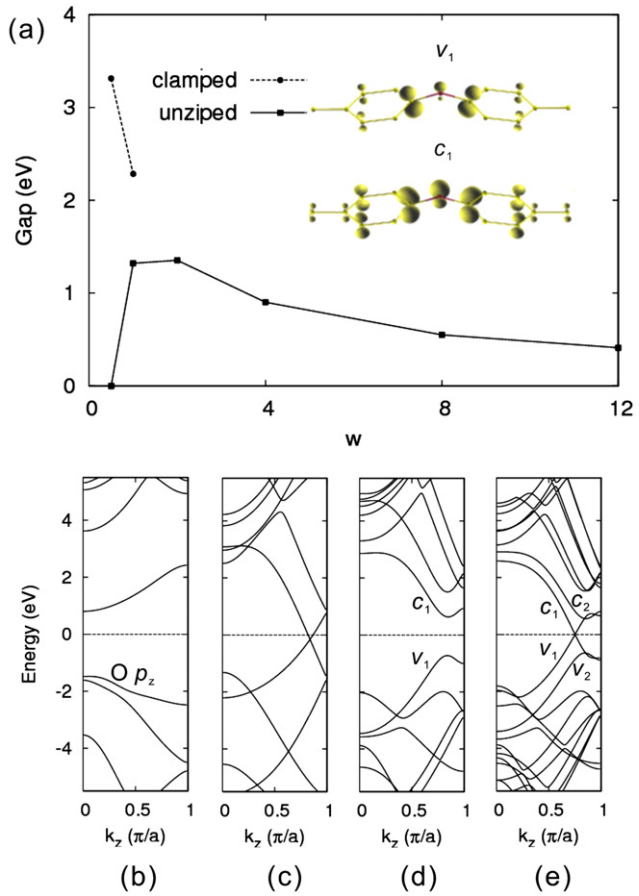

Figure 5. (a) Energy gaps of symmetrically clamped and unzipped graphene epoxide with dependence on width w. Insets: charge density distribution for the first valence (v_1) and conduction bands (c_1) of symmetrically unzipped structure C_8O_{sym}. (b)–(d) show band structures for symmetrically clamped C_4O_{sym} ($w = 1$), symmetrically unzipped C_2O_{sym} ($w = 0.5$), C_8O_{sym} ($w = 2$) and antisymmetrically unzipped C_8O_{asym} ($w = 2$) structures, respectively. The energy is shifted so that the Fermi level $E_F = 0$ eV.

(figure 4(d)) shows the C–C bond starts to break at a strain of 0.18, where the oxygen atoms are embedded into the graphene lattice. It is noticeable that, at the breaking strain of pristine graphene and graphene epoxide, the C–C bond along the tensile direction is elongated by 21% and 23%. The close values suggest the strength of the sheets is mainly contributed by the sp^2 carbon bonds and explains why the tensile strength does not change as much as the Young's modulus.

3.4. Electronic structure of graphene epoxide

The binding of epoxy groups also perturbs the electronic structure of graphene epoxide by destroying local π-electron states. Temperature-dependent electrical measurements and Raman spectroscopy revealed the semiconducting behavior of graphene oxides [8, 30]. In the clamped phase, because the C–C bond does not break, so the oxygen atoms adsorbed act as dopants in the graphene lattice. Hybridization between π-bands in graphene and the oxygen 2p orbital opens a gap and introduces a localized oxygen $2p_z$ band as shown in figure 5(b) [11, 16].

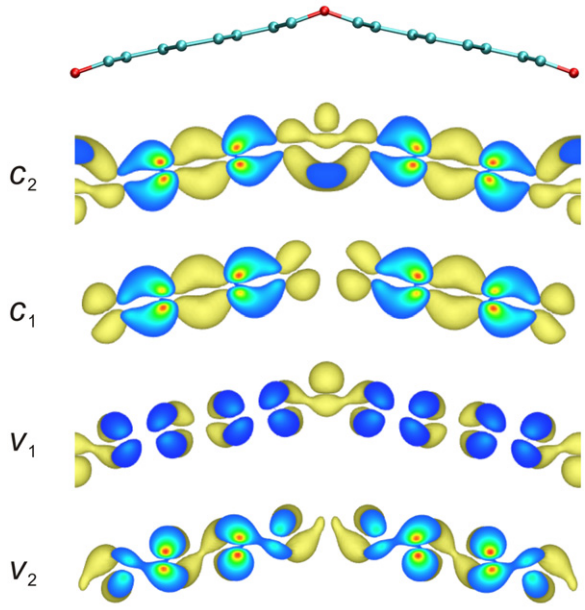

Figure 6. Atomic structure (one unit cell) and electron density plots for C_8O_{asym}. Two valence (v_1, v_2) and two conduction bands (c_1, c_2) close to the Fermi energy (figure 5(e)) are plotted. The density of states is localized in the graphene sheet joined by epoxy groups.

For the unzipped graphene epoxide C_2O ($w = 0.5$), the oxygen atom lies in the graphene lattice and bridges two adjacent carbon atoms. The hybridization between π electrons in oxygen and carbon atoms results in a zero-gap band structure (figure 5(c)) with bands crossing around the Fermi level, while for the unzipped structures with $w \geqslant 1$, epoxy lines cut the graphene into zigzag-edged graphene nanoribbons. Local structural distortion around the epoxy group blocks the π-electron state of graphene (figure 5(d)). The semiconducting gaps opened are inversely proportional to the width of the separated graphene ribbons (figure 5(a)). This dependence reflects the particle-in-a-box nature of the mobile π-state between epoxy barriers and can be explained using the two-band model for graphene. The dispersion relation of the π state in graphene is $E(\mathbf{k}) = \pm\hbar v_F|\mathbf{k}-\mathbf{k}_0|$, where $\mathbf{k}$ is the wavevector and $\mathbf{k}_0$ is the wavevector where the two bands cross. v_F is the Fermi velocity. The energy gap is thus predicted to be $E_g \sim hv_F/w$ and is consistent with our calculation results. It is recently discovered that hydrogen-terminated graphene nanoribbons, edge localized states provide half-metallicity and unique magnetic properties [5]. Electron orbital analysis shows that, in the unzipped structures, the valence v_1 and conduction band c_1 near the Fermi level for $w >= 1$ are localized states at the epoxy group which resemble edge states in graphene nanoribbons (figure 5(a)) [5, 25].

In the antisymmetrically unzipped structures, however, the distortion of a graphene sheet near an epoxy group is negligible. Graphene ribbons hinged by epoxy groups keep their planar sp^2 structure very well. Thus the delocalization of π electrons is maintained and the band structure shows a metallic character, figure 5(e). Figure 6 plots the two valence (v_1, v_2) and conduction (c_1, c_2) bands. These states around the Fermi level are delocalized and contribute to the metallicity.

This can be expected in the symmetric structure only if the graphene ribbon width between epoxy groups is large enough to neglect the effect of edge distortion.

4. Conclusion

In conclusion, we investigated graphene epoxide as an example of engineered graphene materials by functional groups. The focus is placed on their mechanical and electronic properties at various oxidation conditions. For regularly patterned epoxy structures, two phases are revealed to have considerable binding strength consistent with previous experimental observations: the clamped structure where the oxygen adsorbed on the sp^2 bond and the unzipped structure where the epoxy binding breaks the sp^2 bond. The clamped phase presents at high oxidation density and forms a regular lattice, while the unzipped phase is more stable and results in line defects in graphene.

Mechanical properties and electronic structures are studied after the atomic structure is determined. The foldable epoxy structure gives rise to a halving of the Young's modulus, while leaving the tensile strength unaffected. The epoxy group also changes their band structures and results in various electronic properties, depending on the oxidation density and symmetry. These results suggest possible applications such as high strength composites and tunable electronic materials.

Our work lays the groundwork for the design and application of graphene-based functional materials through oxidation control methods, i.e. by altering the epoxidation density and arrangement patterns. The understanding of the structural property relation is also critical for preparing graphene-related materials such as graphene oxide papers [31] through chemical exfoliation methods. Furthermore, with the ability to control the oxidation and reduction process, for example, to modify graphene structure by oxidation in specific regions, one can expect to fabricate tunable graphene-related nanodevices, such as chemical sensors [32] or patternable nano-electric circuits [6, 7]. After submission of this manuscript, we became aware of similar conclusions in a very recent work [33].

References

[1] Novoselov K S, Geim A K, Morozov S V, Jiang D, Zhang Y, Dubonos S V, Grigorieva I V and Firsov A A 2004 Electric field effect in atomically thin carbon films *Science* **306** 666–9

[2] Novoselov K S, Geim A K, Morozov S V, Jiang D, Katsnelson M I, Grigorieva I V, Dubonos S V and Firsov A A 2005 Two-dimensional gas of massless dirac fermions in graphene *Nature* **438** 197–200

[3] Novoselov K S, Jiang Z, Zhang Y, Morozov S V, Stormer H L, Zeitler U, Maan J C, Boebinger G S, Kim P and Geim A K 2007 Room-temperature quantum hall effect in graphene *Science* **315** 1379

[4] Lee C, Wei X, Kysar J W and Hone J 2008 Measurement of the elastic properties and intrinsic strength of monolayer graphene *Science* **321** 385–8

[5] Son Y W, Cohen M L and Louie S G 2006 Half-metallic graphene nanoribbons *Nature* **444** 347–9

[6] Xu Z, Zheng Q-S and Chen G 2007 Elementary building blocks of graphene-nanoribbon-based electronic devices *Appl. Phys. Lett.* **90** 223115

[7] Ci L, Xu Z, Wang L, Gao W, Ding F, Kelly K, Yakobson B and Ajayan P 2008 Controlled nanocutting of graphene *Nano Res.* **1** 116–22

[8] Gómez-Navarro C, Weitz R T, Bittner A M, Scolari M, Mews A, Burghard M and Kern K 2007 Electronic transport properties of individual chemically reduced graphene oxide sheets *Nano Lett.* **7** 3499–503

[9] Tung V C, Allen M J, Yang Y and Kaner R B 2009 High-throughput solution processing of large-scale graphene *Nat. Nano* **4** 25–9

[10] Eda G, Fanchini G and Chhowalla M 2008 Large-Area ultrathin films of reduced graphene oxide as a transparent and flexible electronic material *Nat. Nano* **3** 270–4

[11] Ito J, Nakamura J and Natori A 2008 Semiconducting nature of the oxygen-adsorbed graphene sheet *J. Appl. Phys.* **103** 113712–5

[12] Berger C *et al* 2004 Ultrathin epitaxial graphite: 2d electron gas properties and a route toward graphene-based nanoelectronics *J. Phys. Chem.* B **108** 19912–6

[13] Yang X, Dou X, Rouhanipour A, Zhi L, Räder H J and Müllen K 2008 Two-dimensional graphene nanoribbons *J. Am. Chem. Soc.* **130** 4216–7

[14] Jeong H, Lee Y P, Lahaye R J W E, Park M H, An K H, Kim I J, Yang C, Park C Y, Ruoff R S and Lee Y H 2008 Evidence of graphitic AB stacking order of graphite oxides *J. Am. Chem. Soc.* **130** 4213–5

[15] Stankovich S, Dikin D A, Piner R D, Kohlhaas K A, Kleinhammes A, Jia Y, Wu Y, Nguyen S T and Ruoff R S 2007 Synthesis of graphene-based nanosheets via chemical reduction of exfoliated graphite oxide *Carbon* **45** 1558–65

[16] Boukhvalov D W and Katsnelson M I 2008 Modeling of graphite oxide *J. Am. Chem. Soc.* **130** 10697–701

[17] McAllister M J *et al* 2007 Single sheet functionalized graphene by oxidation and thermal expansion of graphite *Chem. Mater.* **19** 4396–404

[18] Li J-L, Kudin K N, McAllister M J, Prud'homme R K, Aksay I A and Car R 2006 Oxygen-driven unzipping of graphitic materials *Phys. Rev. Lett.* **96** 176101–4

[19] Pandey D, Reifenberger R and Piner R 2008 Scanning probe microscopy study of exfoliated oxidized graphene sheets surface *Science* **602** 1607–13

[20] Lerf A, He H, Forster M and Klinowski J 1998 Structure of graphite oxide revisited *J. Phys. Chem.* B **102** 4477–82

[21] Schniepp H C, Li J-L, McAllister M J, Sai H, Herrera-Alonso M, Adamson D H, Prud'homme R K, Car R, Saville D A and Aksay I A 2006 Functionalized single graphene sheets derived from splitting graphite oxide *J. Phys. Chem.* B **110** 8535–9

[22] Cai W *et al* 2008 Synthesis and solid-state NMR structural characterization of 13c-labeled graphite oxide *Science* **321** 1815–7

[23] Alexandre S S, Mazzoni M S C and Chacham H 2008 Edge states and magnetism in carbon nanotubes with line defects *Phys. Rev. Lett.* **100** 146801–4

[24] Rappe A M, Rabe K M, Kaxiras E and Joannopoulos J D 1990 Optimized pseudopotentials *Phys. Rev.* B **41** 1227–30

[25] Son Y W, Cohen M L and Louie S G 2006 Energy gaps in graphene nanoribbons *Phys. Rev. Lett.* **97** 216803–4

[26] Heyd J and Scuseria G E 2004 Efficient hybrid density functional calculations in solids: assessment of the Heyd–Scuseria–Ernzerhof screened Coulomb hybrid functional *J. Chem. Phys.* **121** 1187–92

[27] Buchsteiner A, Lerf A and Pieper J 2006 Water dynamics in graphite oxide investigated with neutron scattering *J. Phys. Chem.* B **110** 22328–38

[28] Tersoff J and Hamann D R 1985 Theory of the scanning tunneling microscope *Phys. Rev.* B **31** 805–13

[29] Paci J T, Belytschko T and Schatz G C 2007 Computational studies of the structure, behavior upon heating, and mechanical properties of graphite oxide *J. Phys. Chem.* C **111** 18099–111

[30] Gilje S, Han S, Wang M, Wang K L and Kaner R B 2007 A chemical route to graphene for device applications *Nano Lett.* **7** 3394–8

[31] Dikin D A, Stankovich S, Zimney E J, Piner R D, Dommett G H B, Evmenenko G, Nguyen S T and Ruoff R S 2007 Preparation and characterization of graphene oxide paper *Nature* **448** 457–60

[32] Schedin F, Geim A K, Morozov S V, Hill E W, Blake P, Katsnelson M I and Novoselov K S 2007 Detection of individual gas molecules adsorbed on graphene *Nat. Mater.* **6** 652–5

[33] Jia-An Y, Lede X and Chou M Y 2009 Structural and electronic properties of oxidized graphene *Phys. Rev. Lett.* **103** 086802–4